EUROPEAN MECHANICAL SCIENCE

Research Article

e-ISSN: 2587-1110

Investigation of the influence of tartaric acid quantity and calcination temperature on the morphology, crystal structure, and photocatalytic activity of zinc oxide nanoparticles

Mücahid Özcan[1], Serra Ersoy[2*], Figen Kaya[2], Cengiz Kaya[2]

[1]Oak Ridge National Laboratory, Department of Chemical and Materials Sciences, Oak Ridge, Tennessee/US
[2]Yildiz Technical University, Department of Metallurgical and Materials Engineering, 34220, Istanbul/Türkiye

Abstract: In this research article, using zinc acetate dihydrate and tartaric acid, six distinct zinc oxide (ZnO) nanoparticles were synthesized with the sol-gel method to assess the effects of varying the amount of tartaric acid (0.1, 0.05, and 0.01 moles) and the calcination temperatures (400, 500, and 600°C) on the features of morphological, crystal structure, and photocatalytic activity. Moreover, to understand the effect of tartaric acid on photocatalytic activity, UV-visible spectrophotometer analysis was performed by keeping ZnO nanoparticles calcined at 500°C under methylene blue and UV light for 15, 30, 45, 60, 75, and 90 minutes. According to the analysis results, raising the tartaric acid moles generates ZnO nanoparticles with a finer and more uniform prismatic shape; it additionally minimizes the porosity of the particles, which decreases the photocatalytic activity. As a result of this, ZnO nanoparticles prepared with 0.05 mol of tartaric acid have the ultimate photocatalytic activity and promote the destruction of over 94.51% of methylene blue in just 90 minutes. The ZnO nanoparticles developed in this study will likely be employed in surface coatings since they do not harm organic materials or human health, are long-lasting, and use light energy to trigger a chemical reaction.

Keywords: transition metal oxide, tartaric acid, sol-gel method, photochemical material.

1. Introduction

UV or visible light-driven photocatalysis is an effective method for starting chemical reactions that are relevant to the environment [1-3]. Increasing photocatalytic efficiency has been made possible by nanotechnology, especially with the use of semiconductor nanomaterials [4]. Zinc oxide (ZnO), one of the transition metal oxides, has garnered a lot of interest because of its advantageous physicochemical characteristics, which include good optical and electrical qualities, high thermal and chemical stability, non-toxicity, and the ability to absorb ultraviolet light [5–8]. Under UV light, ZnO's broad band-gap semiconductor (3.37 eV) and high exciton binding energy (60 meV) allow for effective electron–hole pair production [9,10]. A wide variety of organic and inorganic contaminants can be broken down more easily when the photogenerated charge carriers go to the surface and take part in redox processes [9,12]. ZnO-based photocatalysts, which frequently display simultaneous photocatalytic, self-cleaning, and antibacterial capabilities, have thus been extensively studied for environmental remediation applications, such as air purification and wastewater treatment [2,11,13–15]. For the production of ZnO nanoparticles, several synthesis pathways have been explored, such as co-precipitation, hydrothermal processing, combustion, and sol-gel techniques. Among them, the sol-gel method is still very appealing because of its ease of use, low processing temperature, compositional control, and capacity to create high-purity, chemically homogenous nanomaterials [12,16–18].

Tartaric acid ($C_4H_3O_4$) was used in this study as a sur-

*Corresponding author:
Email: serra.ersoy@yildiz.edu.tr

© Author(s) 2025. This work is distributed under https://creativecommons.org/licenses/by/4.0/

Cite this article as:
Özcan, M. *et.al.* (2025). Investigation of the influence of tartaric acid quantity and calcination temperature on the morphology, crystal structure, and photocatalytic activity of zinc oxide nanoparticles. *European Mechanical Science*, 9(4): 335-344. https://doi.org/10.26701/ems.1825160

History dates:
Received: 17.11.2025, Revision Request: 13.12.2025, Last Revision Received: 22.12.2025, Accepted: 25.12.2025

face-modifying and structure-directing agent during the sol–gel production of ZnO nanoparticles. Tartaric acid provides an ecologically safe production pathway while successfully influencing nucleation, development, and morphology due to its high water solubility and potent chelating capacity toward Zn^{2+} ions [2,8,18]. The structural, morphological, and photocatalytic characteristics of ZnO nanoparticles are methodically examined in relation to tartaric acid modification and calcination temperature. This work contributes to the logical design of effective ZnO-based photocatalysts for environmental applications and sheds light on the links between shape and activity.

This work examined the impact of calcination temperatures on the morphological, structural, and photocatalytic properties of ZnO nanoparticles treated with tartaric acid. A novel experimental investigation was planned because there isn't another study in the literature that compares tartaric acid and calcination temperature at the same time. Given the numerous uses of ZnO-based photocatalysts in environmental remediation, especially in the breakdown of organic pollutants and wastewater treatment, it is essential to comprehend how tartaric acid improves photocatalytic performance in order to optimize ZnO nanoparticles for useful applications. Furthermore, it is expected that high performance can be attained using a sustainable, non-toxic, and ecologically friendly synthesis technique by comprehending the photocatalytic activity of green-synthesized ZnO nanoparticles, such as those containing tartaric acid. The objective was to determine the ideal calcination and tartaric acid molar ratio in order to perform research that would be used as a reference for subsequent investigations.

2. Materials and Methods

2.1. Materials

Zinc acetate dihydrate ($(CH_3COO)_2Zn$ * 2 H_2O, Merck KGaA /Germany) as the zinc source, tartaric acid ($C_4H_6O_6$, Merck 100804 L(+)-Tartaric Acid for Analysis Emsure®) as the acid and distilled water (DW) were used as a solvent while preparing the solution.

2.2. Methods

In this study, the synthesis of ZnO nanostructures was carried out utilizing the sol-gel method. The experimental groups shown in *Table 1* were created to synthesize six different ZnO NPs. In the experimental study, two different groups were carried out to examine the morphological and structural effects of tartaric acid and calcination temperature on the ZnO NPs.

The experimental procedures depicted in *Figure 1* were carried out in accordance with the schematic representation. Zinc acetate dihydrate and tartaric acid were carefully weighed using a precision balance for each of the three powders of the Exp. 1.0 group, keeping a 1:1 molar ratio, in order to comprehend the impact of calcination temperature. In this experiment, zinc acetate dihydrate was first introduced and dissolved in 100 milliliters of pure water using a magnetic stirrer before tartaric acid was added to a beaker. For 30 minutes at 90 °C, the solution was agitated in a magnetic stirrer at a steady 450 rpm. After that, the mixture was moved to a container after being poured over waxed paper. For a whole day, the sample was dried at 80 °C. Afterwards, to investigate the effect of temperature, it was subjected to heat treatment for one hour at three different calcination temperatures: 400, 500, and 600 °C. Only the calcination temperature was optimized in this experimental group, and the tartaric acid molar ratio was maintained at 0.15 mol. The second experimental group altered the molar ratios of tartaric acid while maintaining a constant calcination temperature of 500 °C. The temperature that produced the best morphological results in the first group was determined to be 500 °C. Additionally, four distinct tartaric acid concentrations were photochemically compared with the powder obtained at 0.15 mol since 0.1, 0.05, and 0.01 moles were to be compared at 500 °C (*Figure 1(c)*).

X-ray diffraction (XRD), the materials were scanned using a ceramic X-ray tube and 1.54 wavelength copper anode radiation from a D8 Advance Bruker XRD for crystallographic phase analysis. Micro-regions, morphological features, and ZnO nanoparticles were investigated using a Zeiss Ultra 55 Gemini device equipped with a deep scanning electron microscope (SEM) at working distances of 15–36 mm and acceleration volt-

Table 1. Chemical ratios of raw materials and different calcination parameters for different ZnO nanoparticles.

Experiment Code	Zinc Source and Moles	Tartaric Acid Moles	Mixing	Drying	Calcination
Exp. 1.0-a	Zinc Acetate Dihydrate (0.15 mole)	0.15	90 °C, 3 hours	80 °C, 24 hours	400 °C, 1 hour
Exp. 1.0-b	Zinc Acetate Dihydrate (0.15 mole)	0.15	90 °C, 3 hours	80 °C, 24 hours	500 °C, 1 hour
Exp. 1.0-c	Zinc Acetate Dihydrate (0.15 mole)	0.15	90 °C, 3 hours	80 °C, 24 hours	600 °C, 1 hour
Exp. 1.1	Zinc Acetate Dihydrate (0.1 mole)	0.1	90 °C, 3 hours	80 °C, 24 hours	500 °C, 1 hour
Exp. 1.2	Zinc Acetate Dihydrate (0.1 mole)	0.05	90 °C, 3 hours	80 °C, 24 hours	500 °C, 1 hour
Exp. 1.3	Zinc Acetate Dihydrate (0.1 mole)	0.01	90 °C, 3 hours	80 °C, 24 hours	500 °C, 1 hour

ages of 3–5 kV. A Shimatzu DTG 60H DTA equipment was used to conduct thermogravimetric and differential thermal analysis (TG/DTA) to investigate temperature variations over time in a sample's physical characteristics [19]. Following UV exposure, 2 ml of methylene blue was added to the ZnO nanoparticles in the quartz bath. In Experiments 1.0-b, 1.1, 1.2, and 1.3, the absorption peaks of the samples between 200 and 800 nm

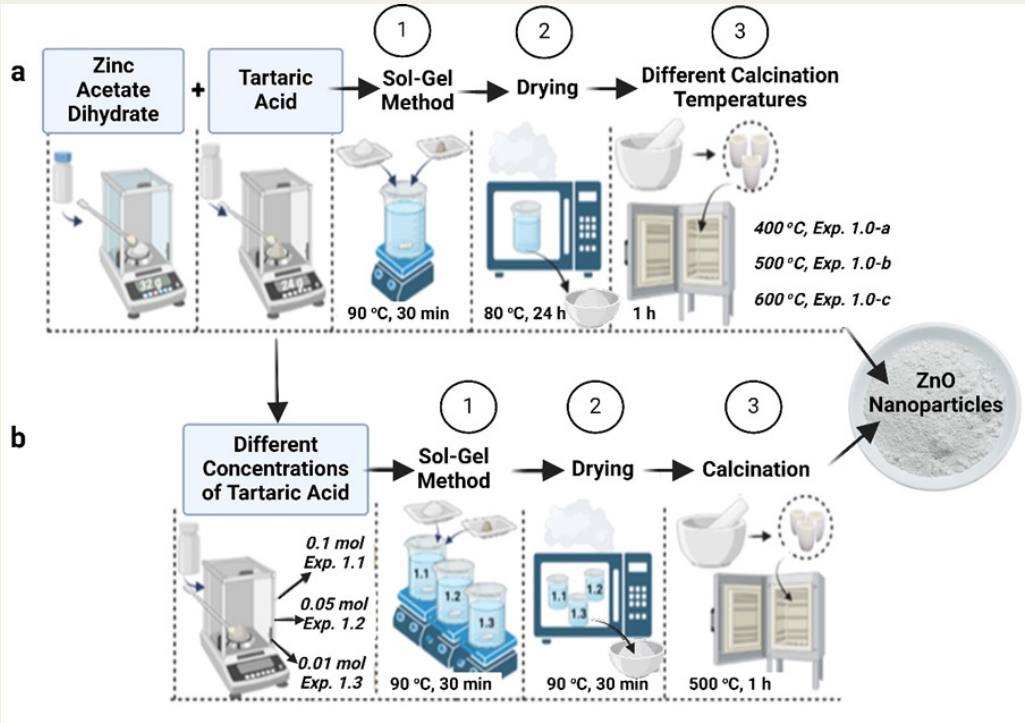


Figure 1. Experiments were carried out by keeping the zinc source constant and changing the **a)** calcination temperatures like 400, 500 and 600 °C and **b)** tartaric acid moles like 0.1, 0.05 and 0.01.

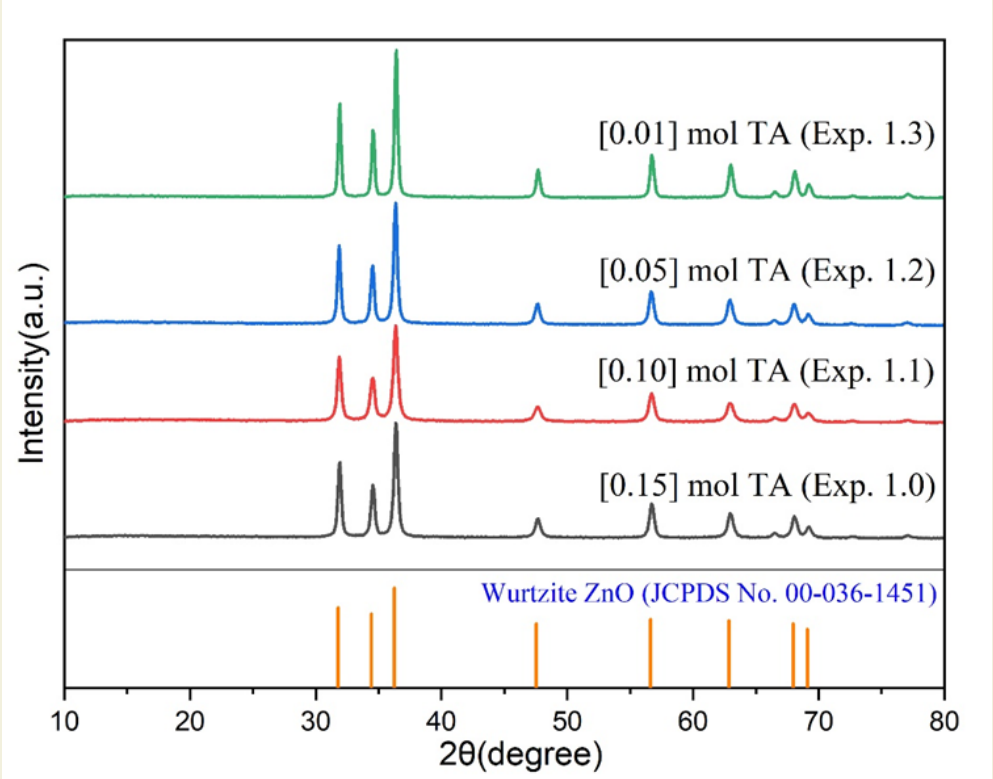


Figure 2. XRD patterns of ZnO nanoparticles synthesized with different tartaric acid moles.

were analyzed under light for different durations using a Cary 5000 UV/Vis/NIR Spectrophotometer for photocatalytic performance of six different ZnO NPs powders [20–25].

3. Results and Discussions

3.1. XRD

The Figure 2 displays the XRD patterns for the produced ZnO NPs. The hexagonal wurtzite structure in the produced ZnO nanoparticles is strongly supported by XRD investigation [24]. The Joint Committee on Powder Diffraction Standards (JCPDS) database indicates that the hexagonal wurtzite structure is formed by the diffraction peaks seen in the planes (100), (002), (101), (102), (110), (103), (200), (112), (201), (004), (202). The peaks corresponding to the planes (100), (002), and (101) in Experiment 1.3 have the highest intensities when the black line representing Experiment 1.0-b, the red line representing Experiment 1.1, the blue line representing Experiment 1.2, and the green line representing Experiment 1.3 are analyzed. It is thought that the observed high peaks may be related to the crystallite growth behavior influenced by the lower tartaric acid content. Zinc ions were shown to interact significantly with carbonyl ions throughout the production process. Tartaric acid's many carboxyl groups are responsible for this interaction. This interaction is especially important for the regulated release of zinc ions and the promotion of ZnO production. Furthermore, the growth and nucleation rate of nanoparticles are also impacted by this interaction. Changes in molar amount determine how tartaric acid affects the crystallization process. A higher molar concentration of tartaric acid promotes nucleation, which results in the creation of tiny particles. Thus, it is evident how nucleation and growth rate affect the crystallinity of nanoparticles [24, 25].

3.2. SEM

The acquired SEM images are shown in Figure 3. The ZnO powders was roughly 360 nm in size, according to the SEM study with ImageJ software. To thoroughly examine the morphological structure, a comparative investigation was carried out at three distinct temperatures. After being calcined at 400 °C, ZnO nanoparticles have a unique shape with sharp edges and a rod-like structure. When nanoparticles were calcined at 500 °C, their porosity dramatically increased but their particles size decreased. The formations that have been discovered show a variety of morphologies, including spherical, branching, and floral patterns. As mentioned in reference [21], the structure's intrinsic porosity is the reason for the lack of sharpness and clarity. The presence of rod-shaped formations with remarkable characteristics in terms of distinctiveness and corner sharpness was discovered through investigation at a high temperature of 600 °C. Nanoparticles calcined at 500 °C were found to have the ideal size, averaging less than 1 micrometer which is 0.257 micrometer approximately [21–23]. Experiments 1.1, 1.2, and 1.3, which varied tartaric acid moles while maintaining constant calcination temperatures, are depicted in Figure 3's SEM pictures. The intriguing finding of porous, irregular, rod-shaped nanoparticles emerging within amorphous formations coexisting with crystalline zinc oxide structures is explained in Experiment 1.1 with Figure 3(d). The overall strength of the aforementioned structures gradually increased in Experiment 1.2 with Figure 3(e). It should be mentioned, nevertheless, that the crystal lattice's struc-

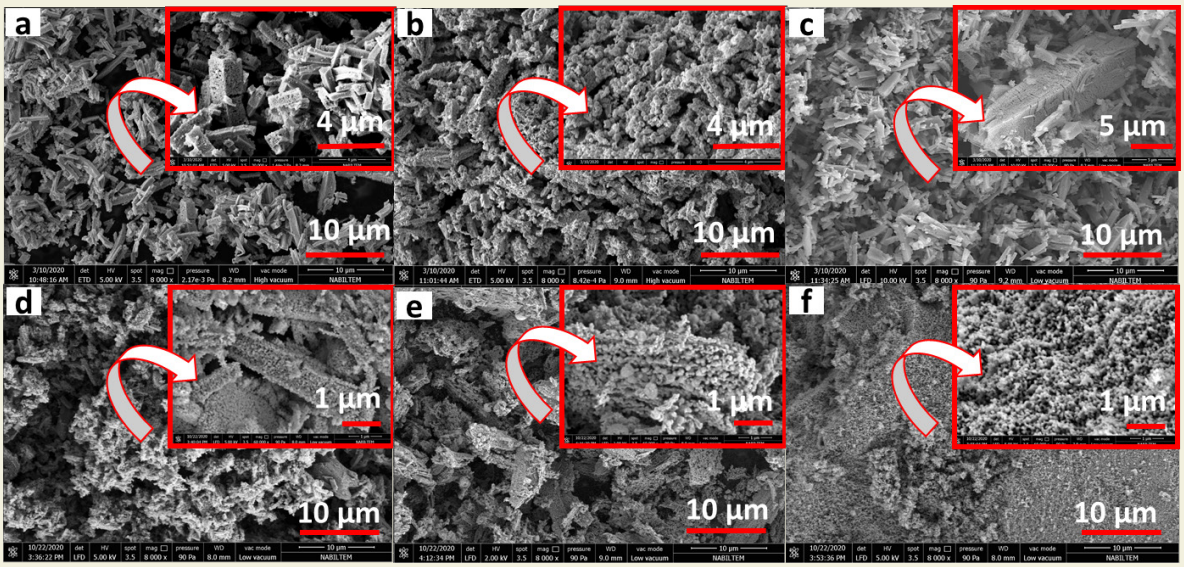


Figure 3. SEM images a) for Exp. 1.0-a, calcination at 400 °C in 4 µm and 10 µm; b) for Exp. 1.0-b, calcination at 500 °C in 4 µm and 10 µm; c) for Exp. 1.0-c, calcination at 600 °C in 5 µm and 10 µm; d) for Exp. 1.1, (0,1) mole tartaric acid in 1 µm and 10 µm; e) for Exp. 1.2, (0,05) mole tartaric acid in 1 µm and 10 µm; f) for Exp. 1.3, (0,01) mole tartaric acid in 1 µm and 10 µm.

tural integrity also decreased at the same time. The decreased molarity of tartaric acid in Experiment 1.3 hindered the observation of flat, rod-shaped nanoparticle formations with Figure 3(f). The substantial dilution of the solution and the ensuing amorphous accumulations were the reasons for the lack of rod development. The existence of residual carbon is most likely the cause of this phenomena. Tartaric acid has been shown to function as a structure-guiding agent when added to a zinc solution. Specifically, it demonstrates the capacity to adsorb the ZnO crystal's polar plane. The observed phenomena is a rise in lateral expansion, and the molarity of tartaric acid determines the morphology that results. In particular, prior research has shown that an increase in the moles of tartaric acid causes more regular, rod-like structures to form [18, 24-30].

The evolution of grain size in the existing system most definitely does not follow a monotonous trend, despite the fact that grain growth normally increases with increasing temperature. Grain growth is still kinetically limited at 500 °C, but the system is dominated by enhanced nucleation and full crystallization. As a result, more nuclei with restricted growth and a smaller average particle size are formed. The observed rise in particle size is explained by enhanced atomic diffusion and grain boundary mobility at higher temperatures, which encourage grain coarsening through sintering and Ostwald ripening mechanisms. Therefore, at 400 °C, there is insufficient nucleation, at 500 °C, there is high nucleation and regulated growth, and at 600 °C, there is intensive growth and sintering. The literature explains that this kind of behavior depends on the equilibrium between temperature, nucleation, and growth [31].

3.3. TG/DTA

The impact of tartaric acid content on the thermal stability of ZnO nanoparticles made using the sol-gel process was examined using TGA analysis in Figure 4. When compared to earlier tests, Experiment 1.3 (0.01 mol), which was carried out by lowering the quantity of tartaric acid employed in the first stage, exhibits notable variations. The observed phenomena is a reduction in the creation of carbon residues and the alteration of the ZnO crystal structure as a result of the reduction in tartaric acid. For experiment 1.3, the breakdown of moisture, salt, and contaminants was noted at a particular temperature of 50 °C during the first stage of decomposition, which takes place in the temperature range of 25 to 250 °C. However, this breakdown process takes place at temperatures higher than 200 °C for different tartaric acid ratios. A notable mass drop was then noted at temperatures between 250 and 350 °C, which coincided with the start of ZnO changes. On the other hand, both mass reduction and transforma-

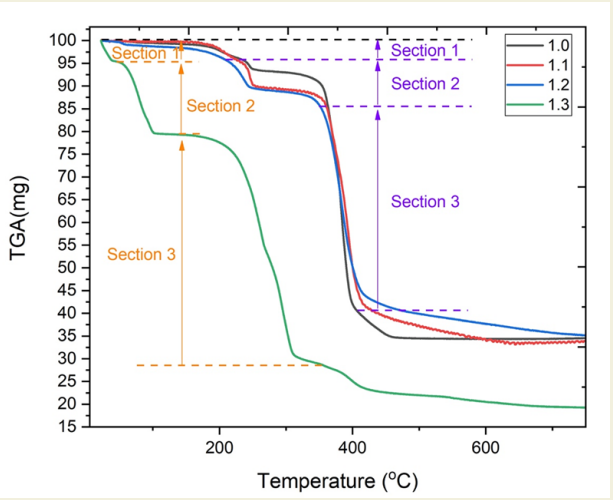


Figure 4. TGA analysis for ZnO nanoparticles with different tartaric acid moles before the calcination process.

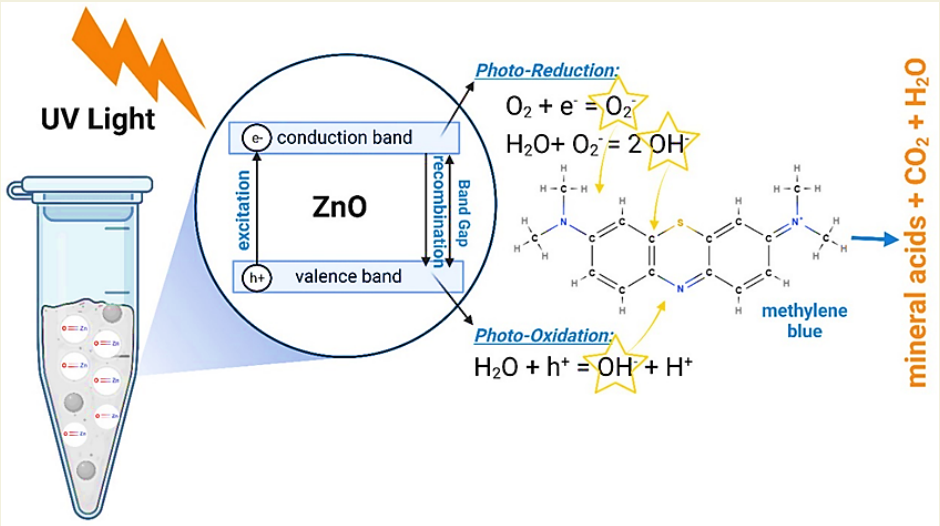


Figure 5. Schematic illustration of photocatalysis mechanism for ZnO nanoparticles.

tion exhibited a declining trend at temperatures above 350 °C, reaching minimal values when ZnO production started. The insufficient presence of tartaric acid was shown to hinder ZnO transformation after the thermal decomposition process in experiment 1.3. Consequently, just 18% of the initial mass was found to be retained. Surprisingly, this reduction was found to be roughly 35% for varying tartaric acid molar concentrations.

3.4. Photocatalytic Activity of ZnO Nanoparticles

ZnO nanoparticles may effectively absorb UV radiation due to their large band gap. Specifically, the photocatalytic process starts with electrons in the valence band gaining energy and moving to the conduction band. Consequently, electron-hole pairs are created as a result of this transition. The absorption of photons with energy levels higher than the band gap promotes the creation of electron-hole pairs. Redox processes are actively carried out by the photogenerated electrons and holes that are produced when photons are absorbed by ZnO nanoparticles. In particular, superoxide radicals are created when electrons in the conduction band perform a reduction process with oxygen molecules (O_2). Concurrently, the valence band's redox gaps promote the oxidation of water molecules (H_2O), which results

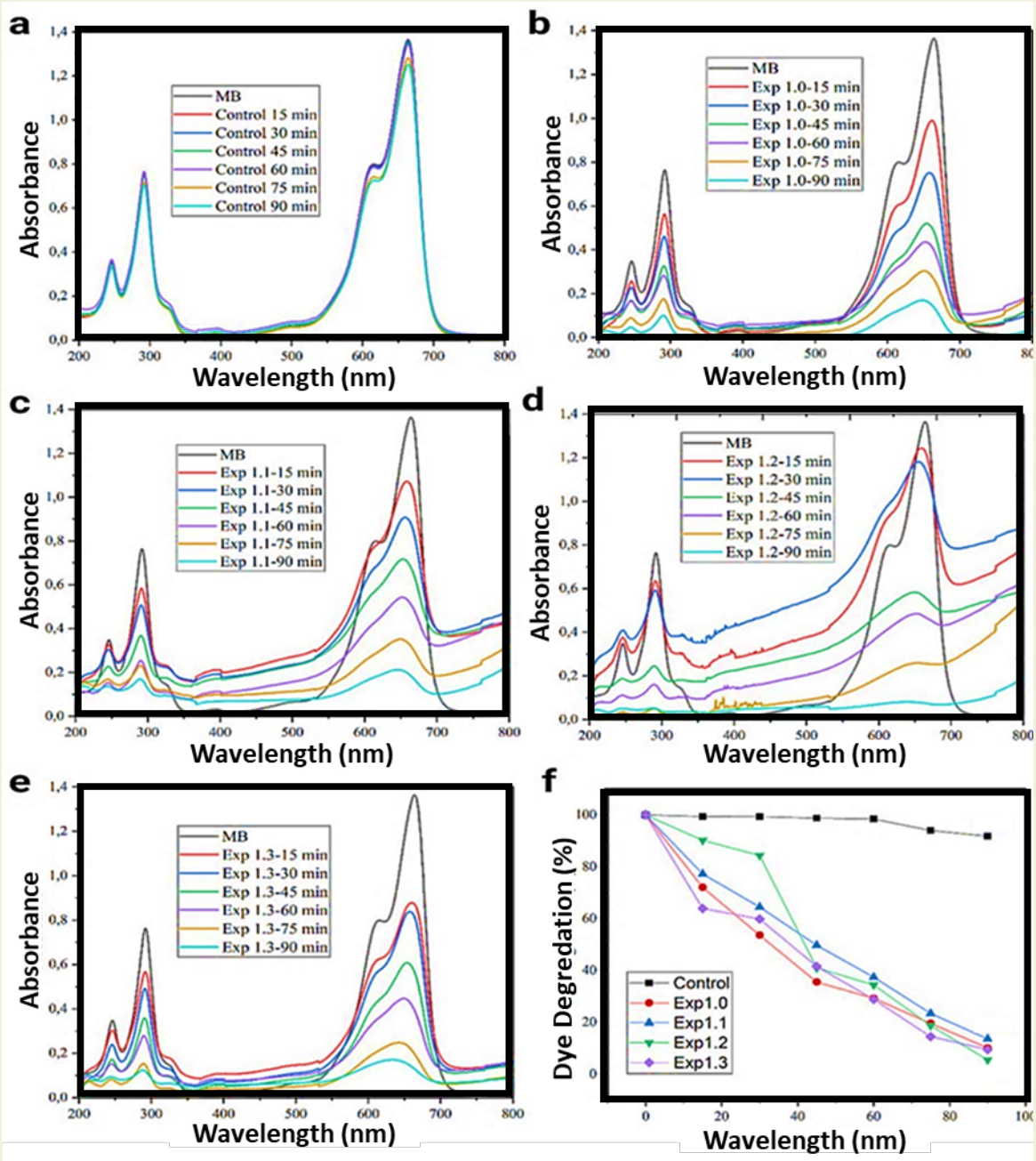


Figure 6. Absorbance peaks of different tartaric acid moles and time for exposure UV radiation of ZnO nanoparticles at between 550-700 nm wavelength: **a)** absorbance peaks of without UV Exp. 1.0, **b)** Exp. 1.0-b, **c)** Exp. 1.1, **d)** Exp. 1.2 and **e)** Exp. 1.3. and **f)** dye degradation (%) of ZnO nanoparticles under ambient conditions.

in the production of hydroxyl radicals (•O.H.) in Figure 5 [26, 28, 29].

The morphology and crystal structure of ZnO nanoparticles produced in varying moles of tartaric acid are depicted in Figure 6, together with the accompanying variations in absorbance in photocatalytic activity. ZnO nanoparticles may break down methylene blue even in the absence of UV light, as seen in Figure 6(a). In approximately 15 minutes, it induced up to 30% disintegration (Figure 6(b)). Measurements taken after the 15-minute limit reveal that methylene blue continues to break down on a regular basis when exposed to UV light; after 90 minutes, the overall breakdown reaches 90%. The decomposition drops from 27.94% to 22.81% when Exp. 1.1 is employed instead of Exp. 1.0-b, as shown in Figure 6(c). This lowers the quantity of methylene blue that decomposes initially because of the loss of ZnO nanoparticle particle homogeneity. The effect of UV light on methylene blue solutions containing ZnO nanoparticles is known to be enhanced by particle homogeneity [28, 29]. The ZnO nanoparticles in Exp. 1.2, which are depicted in Figure 6(d), follow the same principle as the altered particle shape in Exp. 1.1, which decreases photocatalytic activity. As a result, in the first fifteen minutes, the degradation value of Exp. 1.2 drops to 9.83%. It was found that the prismatic ZnO rod shape was broken down and ZnO nanosphere particles were created by progressively raising the molar amount of tartaric acid. The homogenous morphology of the spherical particles totally reverses the decrease in photocatalytic action, even if the rod shape varies [19, 30].

Examining the absorbance values of Experiment 1.3 in Figure 6(e) reveals that the degradation value rises to 36.08% during the first 15 minutes. For Experiment 1.3, the relatively high dye removal (~36%) observed within the first 15 minutes suggests that, given the amorphous or irregular morphology, this initial reduction may be partly due to surface adsorption rather than photocatalytic degradation. Measurements made at 45, 60, 75, and 90 minutes after 30 minutes reveal that Experiment 1.2 degrades methylene blue by about 95% with higher degradation values because of its larger porosity in comparison to other treatments. The experiment's varied dye degradation curves and percentages are displayed in Figure 6(f). The level of pigment degradation of ZnO nanoparticles was found to be at least 86% in the presence of UV light, whereas it did not approach 9% in the absence of UV light. It was determined that 89.89% dye degradation was produced by the particles in experiment 1.0-b being exposed to UV radiation for 90 minutes, 86.4% by the particles in Experiment 1.1, 94.51% by the particles in experiment 1.2, and 90.47% by the particles in Experiment 1.3. To better comprehend the methylene blue decay mechanism of ZnO nanoparticles, Figure 7 displays the decay constant and first-order kinetic calculations and findings. According to the experimental findings, ZnO nanoparticles from Experiment 1.2 demonstrate the strongest photocata-

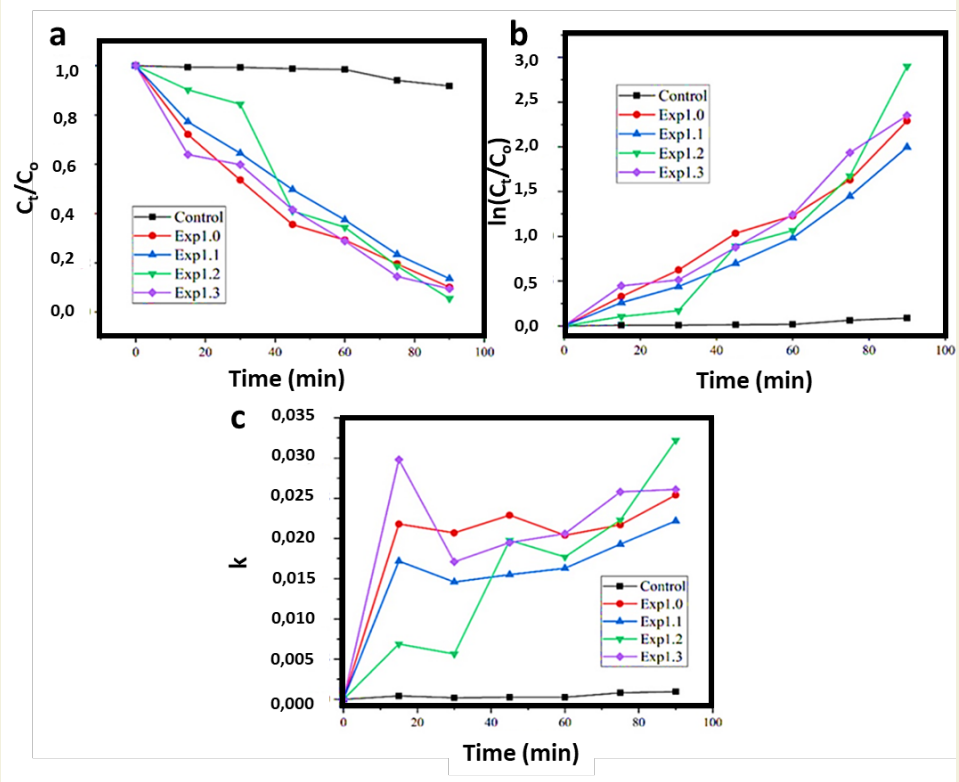


Figure 7. a) Ct/Co ratio of the M.B. dye degradation at different tartaric acid mole ZnO nanoparticles, b) first-order kinetic plots of the M.B. dye degradation, c) and dye degradation rate constants(k).

lytic activity. Ct/Co curves were used to compare how morphological changes affected photocatalytic activity (Figure 7(a)). Experiment 1.2 has a low decay rate (0.8438) at 30 minutes, very near to 1, but Experiment 1.3 has an exceptionally high decay rate (0.6392) after 15 minutes.

By calculating the -ln(Ct/Co) ratio every 15 minutes, decay percentages can be calculated regardless of time (Figure 7(b)). Further proof of its strong photocatalytic activity is the fact that the first-order kinetic graphs of Exp. 1.2 for methylene blue at 75 and 90 minutes are noticeably greater than those of other particles. Exp. 1.3 ZnO nanoparticles have the highest decay coefficient at 15 minutes and the lowest at 90 minutes, according to an analysis of the decay coefficients displayed in Figure 7(c). Additionally, Exp. 1.2 ZnO nanoparticles showed a higher decay coefficient than anticipated after 60 minutes. When exposed to ultraviolet radiation, ZnO nanoparticles containing methylene blue deteriorated, as shown in Figure 8, producing color variations. The control samples' 9% degradation after 90 minutes does not cause a noticeable hue shift. The ZnO nanoparticles produced with different moles of tartaric acid gradient methylene blue become nearly white when subjected to UV light. The methylene blue of Exp. 1.2 ZnO nanoparticles, which degraded the most, is thought to have turned fully transparent after 90 minutes.

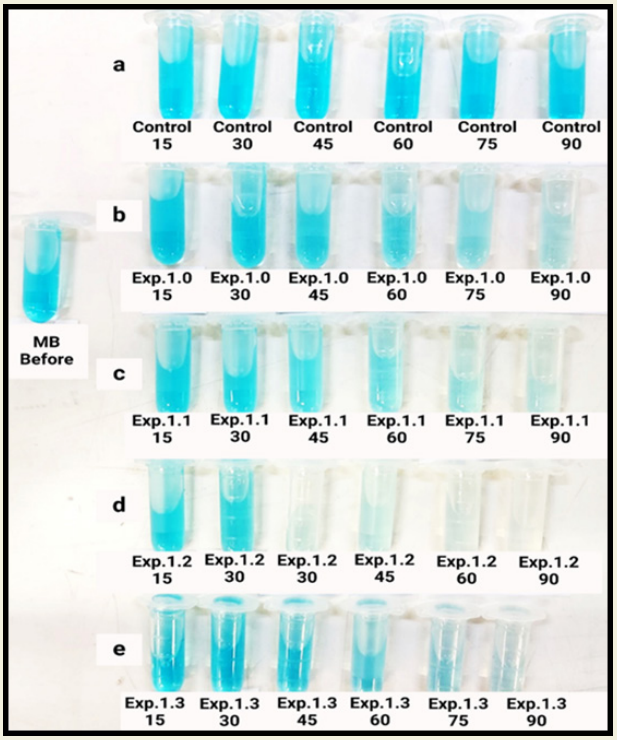


Figure 8. Methylene blue before analysis in UV-visible spectrophotometer to get a baseline and to understand the color change of the ZnO nanoparticle in all experimental groups and the control group at different time intervals **a)** Control group, **b)** Exp. 1.0-b group, **c)** Exp. 1.1 group, **d)** Exp. 1.2 group, and **e)** Exp. 1.3 group.

4. Conclusions

In conclusion, this study examined the effect of tartaric acid and varying calcination temperatures on ZnO nanoparticles in a systematic manner, casting light on the modification of their morphological, structural, and photocatalytic properties. 500 °C is believed to be the optimal calcination temperature for ZnO nanoparticles produced with tartaric acid. Low tartaric acid (0.01 mole.L^{-1}) prevents the production of prismatic forms because it cannot provide sufficient substrate for crystallization. While increasing tartaric acid mole results in forming ZnO nanoparticles with a finer and more uniform prismatic shape, it also decreases photocatalytic activity by reducing porosity. Therefore, ZnO nanoparticles produced with 0.05 mole tartaric acid have the highest photocatalytic activity at 500 °C calcination temperature and induce the degradation of nearly 94.51 % of methylene blue within 90 minutes.

Acknowledgments

The authors also acknowledge the financial support from Yıldız Technical University under contract numbers FBA-2024-6093, FDK-2019-3742 and FBA-2023-5301, respectively. TG/DTA and UV-visible analyses were carried out at Sabancı University Nanotechnology Application and Research Center (SUNUM).

Research ethics

The local Institutional Review Board deemed the study exempt from review

Author contributions

Conceptualization: [Mücahid Özcan], Methodology: [Mücahid Özcan], Formal Analysis: [Serra Ersoy], Investigation: [Serra Ersoy], Resources: [Cengiz Kaya], Data Curation: [Serra Ersoy], Writing - Original Draft Preparation: [Serra Ersoy], Writing - Review & Editing: [Mücahid Özcan], Visualization: [Serra Ersoy], Supervision: [Figen Kaya], Project Administration: [Mücahid Özcan], Funding Acquisition: [Cengiz Kaya]

The author(s) have accepted responsibility for the entire content of this manuscript and approved its submission.

Competing interests

The authors declare that they have no known competing financial interests or personal relationships that could have appeared to influence the work reported in this paper.

Research funding

The authors are grateful for the financial support from Yıldız Technical University under contract numbers FBA-2024-6093, FDK-2019-3742 and FBA-2023-5301.

Data availability

The raw data can be obtained on request from the corresponding author.

Peer-review

Externally peer-reviewed.

Orcid

Mücahid Özcan https://orcid.org/0000-0003-2002-0474
Serra Ersoy https://orcid.org/0009-0006-2278-0871
Figen Kaya https://orcid.org/0000-0002-6652-7062
Cengiz Kaya https://orcid.org/0000-0002-2919-2136

References

[1] Rajaboopathi, S., Thambidurai, S.: Synthesis of bio-surfactant based Ag/ZnO nanoparticles for better thermal, photocatalytic and antibacterial activity. Materials Chemistry and Physics (2019). https://doi.org/10.1016/j.matchemphys.2018.11.034

[2] Duo, S., Zhang, L., Zhong, R., Liu, Z., Huang, L., Liu, T., Zhang, Y.: Controllable tartaric acid modified ZnO crystals and their modification–determined optical, superhydrophilic/hydrophilic and photocatalytic properties. Journal of Alloys and Compounds (2018). https://doi.org/10.1016/j.jallcom.2018.07.195

[3] Abed, C., Ali, M.B., Addad, A., Elhouichet, H.: Growth, structural and optical properties of ZnO-ZnMgO-MgO nanocomposites and their photocatalytic activity under sunlight irradiation. Materials Research Bulletin 110, 230–238 (2019)

[4] Cho, J., Lin, Q., Yang, S., Simmons, J.G., Cheng, Y., Lin, E., Yang, J., Foreman, J.V., Everitt, H.O., Yang, W., Kim, J., Liu, J.: Sulfur-doped zinc oxide (ZnO) Nanostars: Synthesis and simulation of growth mechanism. Nano Res. (2012). https://doi.org/10.1007/s12274-011-0180-3

[5] Ba-Abbad, M.M., Kadhum, A.A.H., Bakar Mohamad, A., Takriff, M.S., Sopian, K.: The effect of process parameters on the size of ZnO nanoparticles synthesized via the sol–gel technique. Journal of Alloys and Compounds (2013). https://doi.org/10.1016/j.jallcom.2012.09.076

[6] Kumar, A.: Sol gel synthesis of zinc oxide nanoparticles and their application as nano-composite electrode material for supercapacitor. Journal of Molecular Structure (2020). https://doi.org/10.1016/j.molstruc.2020.128654

[7] Pallavolu, M.R., Nallapureddy, J., Nallapureddy, R.R., Neelima, G., Yedluri, A.K., Mandal, T.K., Pejjai, B., Joo, S.W.: Self-assembled and highly faceted growth of Mo and V doped ZnO nanoflowers for high-performance supercapacitors. Journal of Alloys and Compounds (2021). https://doi.org/10.1016/j.jallcom.2021.161234

[8] Biji, M., Irfana, M.I., Sreejamol, S., Shajesh, P., Ananthakumar, S., Mangalaraja, R.V., Anas, S.: Tartaric Acid Mediated Gelation Synthesis of Zinc Oxide Nanoparticles and their Photocatalytic Activity. Materials Today: Proceedings (2019). https://doi.org/10.1016/j.matpr.2018.10.376

[9] Kondal, N.: Effect of high temperature annealing on structural and defect associated properties on ZnO nanoparticles. Materials Today: Proceedings (2021). https://doi.org/10.1016/j.matpr.2020.09.009

[10] Tabib, A., Bouslama, W., Sieber, B., Addad, A., Elhouichet, H., Férid, M., Boukherroub, R.: Structural and optical properties of Na doped ZnO nanocrystals: Application to solar photocatalysis. Applied Surface Science (2017). https://doi.org/10.1016/j.apsusc.2016.11.204

[11] Ismail, A.M., Menazea, A.A., Kabary, H.A., El-Sherbiny, A.E., Samy, A.: The influence of calcination temperature on structural and antimicrobial characteristics of zinc oxide nanoparticles synthesized by Sol–Gel method. Journal of Molecular Structure (2019). https://doi.org/10.1016/j.molstruc.2019.06.084

[12] Al Abdullah, K., Awad, S., Zaraket, J., Salame, C.: Synthesis of ZnO Nanopowders By Using Sol-Gel and Studying Their Structural and Electrical Properties at Different Temperature. Energy Procedia (2017). https://doi.org/10.1016/j.egypro.2017.07.080

[13] Peña-Garcia, R., Guerra, Y., Farias, B., Buitrago, D.M., Franco, A., Padrón-Hernández, E.: Effects of temperature and atomic disorder on the magnetic phase transitions in ZnO nanoparticles obtained by sol–gel method. Materials Letters (2018). https://doi.org/10.1016/j.matlet.2018.08.148

[14] Sowri Babu, K., Ramachandra Reddy, A., Sujatha, C., Venugopal Reddy, K., Mallika, A.N.: Synthesis and optical characterization of porous ZnO. J Adv Ceram (2013). https://doi.org/10.1007/s40145-013-0069-6

[15] Siddique, M., Fayaz, N., Saeed, M.: Synthesis, characterization, photocatalytic activity and gas sensing properties of zinc doped manganese oxide nanoparticles. Physica B: Condensed Matter (2021). https://doi.org/10.1016/j.physb.2020.412504

[16] Mahdavi, R., Ashraf Talesh, S.S.: The effect of ultrasonic irradiation on the structure, morphology and photocatalytic performance of ZnO nanoparticles by sol-gel method. Ultrasonics sonochemistry (2017). https://doi.org/10.1016/j.ultsonch.2017.05.012

[17] Hasnidawani, J.N., Azlina, H.N., Norita, H., Bonnia, N.N., Ratim, S., Ali, E.S.: Synthesis of ZnO Nanostructures Using Sol-Gel Method. Procedia Chemistry (2016). https://doi.org/10.1016/j.proche.2016.03.095

[18] Suwanboon, S., Amornpitoksuk, P., Randorn, C.: Effect of tartaric acid as a structure-directing agent on different ZnO morphologies and their physical and photocatalytic properties. Ceramics International (2019). https://doi.org/10.1016/j.ceramint.2018.10.116

[19] Retamoso, C., Escalona, N., González, M., Barrientos, L., Allende-González, P., Stancovich, S., Serpell, R., Fierro, J., Lopez, M.: Effect of particle size on the photocatalytic activity of modified rutile sand (TiO2) for the discoloration of methylene blue in water. Journal of Photochemistry and Photobiology A: Chemistry (2019). https://doi.org/10.1016/j.jphotochem.2019.04.021

[20] Jaramillo, A.F., Baez-Cruz, R., Montoya, L.F., Medinam, C., Pérez-Tijerina, E., Salazar, F., Rojas, D., Melendrez, M.F.: Estimation of the surface interaction mechanism of ZnO nanoparticles modified with organosilane groups by Raman Spectroscopy. Ceramics International (2017). https://doi.org/10.1016/j.ceramint.2017.06.027

[21] N. Funda AK AZEM, Işıl BİRLİK: Sol-jel Yöntemi ile Hazırlanmış ZnO Nanopartiküllerin Optimizasyonu. https://doi.org/10.21205/deufmd.

[22] Shoaib, A., Ji, M., Qian, H., Liu, J., Xu, M., Zhang, J.: Noble metal nanoclusters and their in situ calcination to nanocrystals: Precise control of their size and interface with TiO2 nanosheets and their versatile catalysis applications. Nano Res. (2016). https://doi.org/10.1007/s12274-016-1069-y

[23] Ashraf, R., Riaz, S., Kayani, Z.N., Naseem, S.: Effect of Calcination on Properties of ZnO Nanoparticles. Materials Today: Proceedings (2015). https://doi.org/10.1016/j.matpr.2015.11.071

[24] Deepty, M., Srinivas, C., Kumar, E.R., Mohan, N.K., Prajapat, C.L., Rao, T.C., Meena, S.S., Verma, A.K., Sastry, D.L.: XRD, EDX, FTIR and ESR spectroscopic studies of co-precipitated Mn–substituted Zn–ferrite nanoparticles. Ceramics International (2019). https://doi.org/10.1016/j.ceramint.2019.01.029

[25] Golsheikh, A.M., Kamali, K.Z., Huang, N.M., Zak, A.K.: Effect of calcination temperature on performance of ZnO nanoparticles for dye-sensitized solar cells. Powder Technology (2018). https://doi.org/10.1016/j.powtec.2017.11.065

[26] Raj, K.P., Sadayandi, K.: Effect of temperature on structural, optical and photoluminescence studies on ZnO nanoparticles synthesized by the standard co-precipitation method. Physica B: Condensed

Matter (2016). https://doi.org/10.1016/j.physb.2016.01.020

[27] Ungula, J., Dejene, B.F.: Effect of solvent medium on the structural, morphological and optical properties of ZnO nanoparticles synthesized by the sol–gel method. Physica B: Condensed Matter (2016). https://doi.org/10.1016/j.physb.2015.10.007

[28] Kim, S., Park, H., Choi, W.: Comparative Study of Homogeneous and Heterogeneous Photocatalytic Redox Reactions: PW(12)O(40)(3-) vs TiO(2). The journal of physical chemistry. B (2004). https://doi.org/10.1021/jp049789g

[29] Xu, S., Wang, Z.L.: One-dimensional ZnO nanostructures: Solution growth and functional properties. Nano Res. (2011). https://doi.org/10.1007/s12274-011-0160-7

[30] Li, D., Song, H., Meng, X., Shen, T., Sun, J., Han, W., Wang, X.: Effects of Particle Size on the Structure and Photocatalytic Performance by Alkali-Treated TiO2. Nanomaterials (Basel, Switzerland) (2020). https://doi.org/10.3390/nano10030546

[31] Thanh, N. T. K., Maclean, N., & Mahiddine, S. (2014). Mechanisms of nucleation and growth of nanoparticles in solution. Chemical Reviews, 114(15), 7610–7630. https://doi.org/10.1021/cr400544s